

[doi:10.2109/jcersj2.16243](https://doi.org/10.2109/jcersj2.16243)

# Performance and evolution of planar copper-based anode-supported solid oxide fuel cells

**Vincenzo DE MARCO\***, **Alessandro IANNACI\*\***, **Saqib RASHID\*** and **Vincenzo M. SGLAVO\*,\*\***

\*Department of Industrial Engineering, University of Trento, Via Sommarive 9, 38123, Trento, Italy

\*\*INSTM, Trento Research Unit, Via G. Giusti 9, 50121, Florence, Italy

# Performance and evolution of planar copper-based anode-supported solid oxide fuel cells

Vincenzo DE MARCO<sup>\*,†</sup>, Alessandro IANNACI<sup>\*\*</sup>, Saqib RASHID<sup>\*</sup> and Vincenzo M. SGLAVO<sup>\*,\*\*</sup>

<sup>\*</sup>Department of Industrial Engineering, University of Trento, Via Sommarive 9, 38123, Trento, Italy

<sup>\*\*</sup>INSTM, Trento Research Unit, Via G. Giusti 9, 50121, Florence, Italy

The performances of innovative planar copper-based anode supported solid oxide fuel cells were investigated. Li-containing Gadolinia-doped Ceria (GDC) and Lanthanum Strontium Cobalt Ferrite/Li-GDC were used for the electrolyte and the cathode, respectively; anodes consisting of 35 or 45 vol % CuO/GDC were produced and the corresponding green cells were sintered at 950 and 900°C, respectively. Polarization and power density measurements revealed an important dependence of the electrochemical parameters on sintering temperature and anodic composition. Cu redistribution within the anodic cermet during cell operation was investigated and energy dispersive spectroscopy analysis of anode structure before and after operation revealed Cu migration towards the anode/electrolyte interface.

©2017 The Ceramic Society of Japan. All rights reserved.

Key-words : IT-SOFC, Copper-based anode, Li-GDC, Sintering

[Received October 29, 2016; Accepted December 12, 2016]

## 1. Introduction

Solid Oxide Fuel Cells (SOFC) are energy conversion devices which can efficiently operate at different temperature from about 500 to 1000°C.<sup>1–4)</sup> Although the processes and reactions kinetic is faster, several problems are related to the high operating temperature, like high cost of suitable materials, their compatibility and stability. In particular, high temperature operative conditions can be responsible for several problems like catalyst poisoning, thermal instability, stresses due to thermal expansion mismatch and interdiffusion phenomena between electrolyte and electrodes.<sup>5–7)</sup> Such problems have driven the research to focus on the Intermediate Temperature (IT) range (550–750°C).<sup>8–10)</sup> Nowadays, anodes are often made by yttria-stabilized zirconia (YSZ) and Ni. Unfortunately this latter is toxic<sup>11)</sup> and is subject to deactivation by contaminants present in fuels even in limited levels.<sup>12,13)</sup> As a conclusion, the literature review suggests the use of innovative copper-based anode as potential solution to this latter inconvenient.<sup>14)</sup> Recently, new Cu/ceria-based anodes have been developed and successfully tested in tubular and planar cells,<sup>15–17)</sup> showing good electronic conductivity and high poisoning resistance.<sup>14)</sup> Unfortunately, Gadolinia-doped ceria (GDC) shows a high sintering temperature, this being above 1400°C.<sup>18)</sup> Since the IT-SOFCs are produced through one step cosintering, in order to obtain an electrolyte GDC-based gas tight microstructure at temperature compatible with CuO melting point (below 1100°C), Li<sub>2</sub>O has been used as sintering aid for GDC.<sup>18–20)</sup> One important aspect regards the evolution of anode microstructure upon service and, above all, possible copper migration through the electrolyte or its accumulation at the anode/electrolyte interface. This effect has been previously investigated for different Ni/ceramic anodic cermets configurations. Liu et. al report a Ni migration after durability tests and its agglomeration in

Ni/YSZ cermets.<sup>21)</sup> They studied also Ni diffusion in the YSZ electrolyte composition and they found that Ni accounts at 1% wt at the electrolyte/anode interface whereas far from the anode Ni is not present. If the electrolyte employed is not free from impurities, this phenomenon is increased. The enhancement of Ni diffusion is enhanced by the presence of impurities, such as a glass phase, because Ni can dissolve into this phase. They purposed a Ni diffusion mechanism based on NiO formation when glass phase is present in YSZ electrolyte. This has been measured under testing conditions with high water-containing atmosphere and in the central part of the anode. Then, during interruption for measurements and particularly during cooling, there's a decrease of water atmosphere that lowers pO<sub>2</sub> bringing to a Ni reduction and its deposition in the opened grain boundaries cracking the electrolyte. Segregation of Ni in Ni/YSZ systems starts from 1000°C in 97% H<sub>2</sub>/3% H<sub>2</sub>O. Other impurities segregation can also starts during cell operative conditions (850°C) and their damaging effect is improved by the improvement of water concentration. Transportation of Ni in Ni/YSZ systems, from the electrode to the electrolyte, mainly occurs via grain boundary and surface diffusion. Anyway, in Ni/GDC based cermets, V. Gil et. Al. report that the reduction of Ni<sub>2</sub>O to metallic Ni at 700°C doesn't alter anode/electrolyte interface if both of them have similar coefficients of thermal expansion.<sup>22)</sup> On this basis, it is interesting to analyse the copper behaviour within the CuO/GDC based cermet. In the present work, the electrochemical performance of IT-SOFC with different CuO-GDC-based anodic composition was compared and Cu migration within the anodic cermet during cell operation is studied.

## 2. Experimental procedure

Sub-micron 10 mol % gadolinia doped-ceria (GDC10) (Treibacher Industrie AG, d<sub>50</sub> = 0.27 μm, d<sub>90</sub> = 0.40 μm and SSA = 9.10 m<sup>2</sup>/g) and CuO (Sigma Aldrich) powders were used in the present work. LiNO<sub>3</sub> (Avantor Materials, Baker analyzed reagent) was dissolved in distilled water (solvent to powder ratio = 3/1) and the appropriate amount of GDC10 was added to

<sup>†</sup> Corresponding author: V. De Marco; E-mail: vincenzo.demarco@unitn.it

<sup>‡</sup> Preface for this article: DOI <http://doi.org/10.2109/jcersj2.125.P4-1>

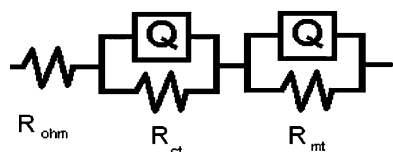


Fig. 1. Equivalent circuit employed for the impedance spectrum evaluation ( $R_{\Omega}$  = ohmic resistance,  $R_{CT}$  = charge transfer resistance,  $R_{MT}$  = mass transfer resistance,  $Q$  = Constant phase element).

achieve a Li-doping concentration of 5 mol %, useful to enhance densification of GDC10. The powder was then calcined at 530°C. Both anode and electrolyte were produced by tape casting (Mistler, Yardley, PA) starting from water-based slurry consisting of solvent (distilled water), dispersant and  $\text{Li}_2\text{O}$ -containing GDC powder, Li being used as sintering aid; 35 or 45 vol % CuO was added to the suspension for producing the anode. Green half-cells were obtained by thermo-pressing (30 MPa, 80°C, 15 min) anode (thickness  $\approx 500\ \mu\text{m}$ ) and electrolyte (thickness  $\approx 50\ \mu\text{m}$ ); the cathode was realized by screen printing using 50 wt % LSCF (Treibacher Industrie, Lot. EA 14/11.2) and 50 wt % GDC powder in ethanol (powder/solvent weight ratio = 1:1).<sup>15)</sup> Two different green cells were therefore produced, whose anode contained 35 or 45 vol % CuO: the two cells were labelled Cu35 and Cu45, respectively and were sintered for 3 h at 950 and 900°C, respectively. The cells were sintered at different temperatures in order to investigate the effect of both the sintering temperature and the cermet composition on the overall SOFC performance. Details of the slurries composition, processing conditions, reduction and electrochemical characterization are reported elsewhere.<sup>15)</sup>

Electrochemical impedance spectroscopy parameters were evaluated at 600°C by employing the equivalent circuit reported in Fig. 1 and using Zsimpwin 3.22 program.

After the electrochemical characterization, some cells were manually but carefully broken to expose a fracture surface orthogonal to the cell plane. The microstructure was analyzed by Scanning Electron Microscopy (SEM) coupled with Energy Dispersive X-ray Spectroscopy (EDS). As shown in Figs. 2(a) and 2(b), the produced fracture surfaces were divided into 9 different sections within the anode thickness, position 1 and 9 corresponding to the outer portion and the anode/electrolyte interface, respectively. Electrolyte thickness has been evaluated using ImageJ 1.5b. For each section, Cu and Ce content was evaluated and comparison was made between cells before and after the electrochemical characterization.

### 3. Results

#### 3.1 Cells performance

Figure 3 shows the electrochemical performance of Cu35 and Cu45 cells at 600°C. OCV is slightly larger than to 0.8 V. Literature reports<sup>23)</sup> that the addition of lithium should not cause any electronic conductivity. Thus, other factors should account for the difference between experimental and theoretical (e.g.: residual leakages in the electrolyte). Despite an higher OCV is expected for Cu35, due to its better electrolyte densification, the OCV of Cu35 and Cu45 is 0.83 and 0.85, respectively. Such limited relative difference (less than 3%) is likely due to some aleatory (e.g.: concentrated losses in Cu35 or difference between the actual and the measured air flow in one or both tests). Both cells achieve power density of  $12\ \text{mW cm}^{-2}$  at current density  $\approx 25\ \text{mA cm}^{-2}$ . Similar polarization and power density curves were obtained for the cells containing different CuO load in the anode and sintered at different temperature. In order to distin-

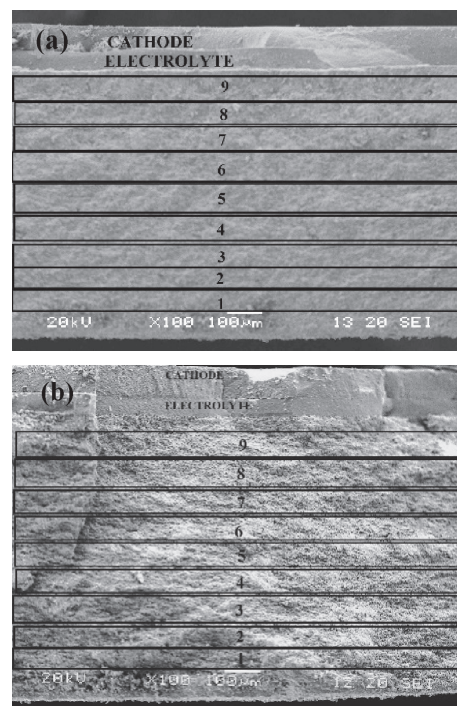


Fig. 2. Fracture surface of (a) 35 vol %<sup>15)</sup> and (b) 45 vol % CuO-containing anode-supported SOFC.

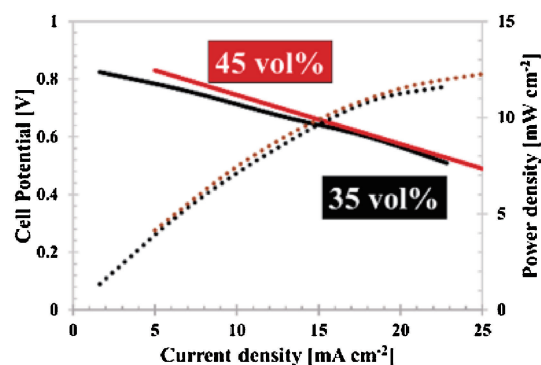


Fig. 3. Electrochemical performance Cu35<sup>11)</sup> and Cu45 SOFC at 600°C.

guish the effect of such parameters Nyquist and Bode plots were recorded as shown in Fig. 4. Two arcs are clear in all spectra. In Nyquist plot [Fig. 4(a)], the electrolyte ohmic resistance ( $R_{\Omega}$ ) is always associated with the first intersection of the curve with the real part axis,<sup>24)</sup> here occurring at about 11 and  $12\ \Omega\text{cm}^2$  for Cu35 and Cu45 cell, respectively. As previously reported,<sup>25)</sup> higher sintering temperature allows to reduce both bulk and grain boundary resistance and, on this basis, it is therefore possible to explain the lower electrolyte ohmic resistance of Cu35 cell. Therefore, regardless the Cu content in the anode, a more densified electrolyte structure accounts for larger ionic GDC conductivity. The estimated electrolyte ohmic resistance is here relatively high, this being related to the fairly large thickness of the GDC membrane (equal to about  $50\ \mu\text{m}$ ). It could be very likely reduced by using different electrolyte fabrication strategies, like, for example, screen printing.<sup>26,27)</sup> Figs. 4(a) and 4(b) provide the electrolyte fracture surface of Cu35 and Cu45, respectively. The checked electrolyte thickness has was  $\approx 55\ \mu\text{m}$  for both cells.

As previously specified, the spectra in Fig. 5 were analyzed according to the equivalent circuit in Fig. 1, where  $R_{CT}$  and  $R_{MT}$

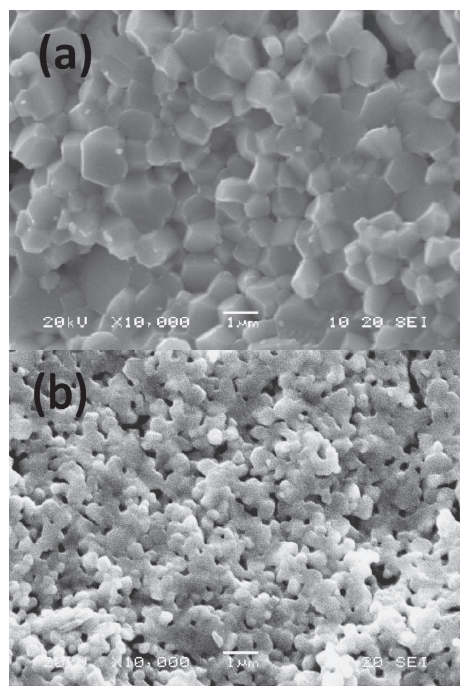


Fig. 4. Electrolyte fracture surface of 35 vol % (a) and 45 vol % CuO-containing anode (b) supported SOFC.

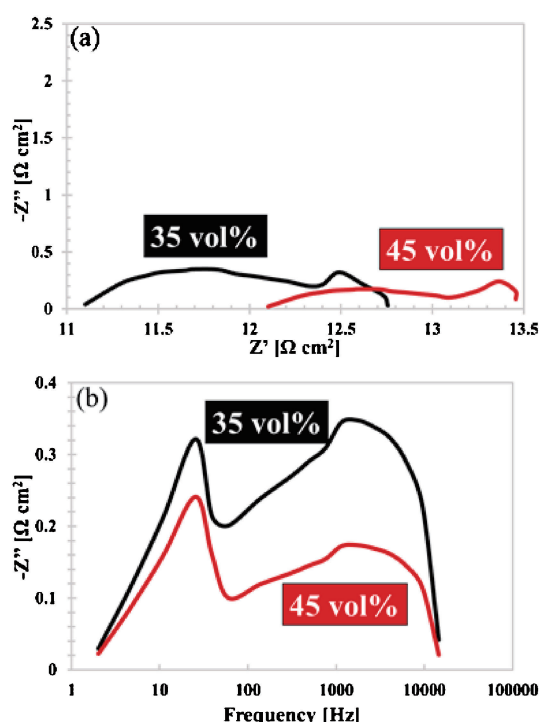


Fig. 5. Nyquist (a) and Bode (b) plot for Cu35<sup>15)</sup> and Cu45 SOFC at 600°C.

are the charge transfer resistance and mass transfer resistance, respectively.<sup>24)</sup>

$R_{CT}$  depends on the hydrogen electro-oxidation and oxygen reduction reactions and it is associated with the high frequency arc in Fig. 5(b).<sup>24)</sup> Conversely,  $R_{MT}$  depends on the gas-transport phenomena occurring at the anode and cathode sides and it is related to the low-frequency arc.<sup>28),29)</sup>

Fitting the plots in Fig. 5 according to the equivalent circuit in

Table 1. Impedance spectra fitting parameters for the two cells at 600°C

|      | $R_{\Omega}$<br>( $\Omega \text{ cm}^2$ ) | $R_{CT}$<br>( $\Omega \text{ cm}^2$ ) | $R_{MT}$<br>( $\Omega \text{ cm}^2$ ) |
|------|---|---------------------------------------|---------------------------------------|
| Cu35 | 11.1                                      | 1.1                                   | 0.6                                   |
| Cu45 | 12.3                                      | 0.7                                   | 0.5                                   |

Table 2. EDX quantitative analysis results for Cu35 and Cu45 anode before and after the reduction

| Anode CuO content<br>(vol %) | Copper concentration [wt %] |           |                 |           |
|------------------------------|-----------------------------|-----------|-----------------|-----------|
|                              | Before reduction            |           | After reduction |           |
|                              | Section 1                   | Section 9 | Section 1       | Section 9 |
| 35                           | 33                          | 31        | 27              | 44        |
| 45                           | 40                          | 39        | 35              | 45        |

Fig. 1, the three resistances ( $R_{\Omega}$ ,  $R_{CT}$  and  $R_{MT}$ ) can be estimated as reported in **Table 1**. In agreement with previous observation,  $R_{\Omega}$  decreases of  $\approx 10\%$  from Cu35 to Cu45 cell, this pointing out a better electrolyte densification in the SOFC sintered at higher temperature. The impedance analysis reveals that, for this specific case, the electrolyte ohmic resistance is predominant ( $\approx 11$ – $12 \Omega \text{ cm}^2$ ) in comparison to the losses associated with the electrodes (less than  $1 \Omega \text{ cm}^2$ ). Therefore, the anode composition does not significantly affect the ohmic resistance, this being mainly due to the electrolyte.<sup>24),30)</sup>

The polarization resistances,  $R_{CT}$  and  $R_{MT}$ , decrease in Cu45. In particular,  $R_{CT}$  decrease with the Cu content, while  $R_{MT}$  decreases with lowering the sintering temperature, due to the increase in the porosity of anode. For 35 vol % CuO – containing anode,  $R_{CT}$  is equal to  $1.1 \Omega \text{ cm}^2$  and decreases down to  $0.7 \Omega \text{ cm}^2$  by increasing the Cu content. In the Cu-GDC anode formulation considered in the present work, using pure  $\text{H}_2$  as anodic fuel, the catalytic activity towards  $\text{H}_2$  oxidation reaction has been ascribed to  $\text{Cu}^0$ , while ceria provides creation of oxygen vacancies.<sup>31)</sup> Therefore, despite 35 vol % CuO is enough to realize an operating electrode, larger CuO load is responsible for more efficient electrons mobility within the anode, this reducing the charge transfer phenomena.<sup>14)</sup> One can therefore conclude that, regardless the sintering temperature, larger Cu load in the anode is responsible for lower charge transfer resistance. On the other hand, the mass transfer resistance appears independent on both sintering temperature and CuO concentration in the anode, the mass transfer phenomena being much more influenced by temperature variations, as previously reported.<sup>28)</sup>

### 3.2 Anodes SEM/EDS characterization

Cu and Ce content was measured on SOFC fracture surface in correspondence of the anode as specified before. **Table 2** compares the results obtained on section 1 and 9, before and after the operation. In the former case, Cu concentration is substantially constant in the two considered sections; this demonstrates a homogeneous Cu distribution in the anode ( $\approx 32\%$  and  $\approx 40\%$  for Cu35 and Cu45 cells, respectively).

Conversely, after cells operation, a relatively large difference in copper concentration between the considered sections can be pointed out, suggesting a certain diffusion within the anode during cell operation. For Cu35 anode, copper content decreases from 33 to 27% in section 1 after the operation, this corresponding to a relative difference of about 18%. The effect is even more evident in section 9 where Cu concentration increases from 31 to 44 wt %, corresponding to a relative increment of  $\approx 42\%$ . For Cu45 anode, the relative difference in section 1 and 9 is  $\approx -12.5 \text{ wt } \%$ , and



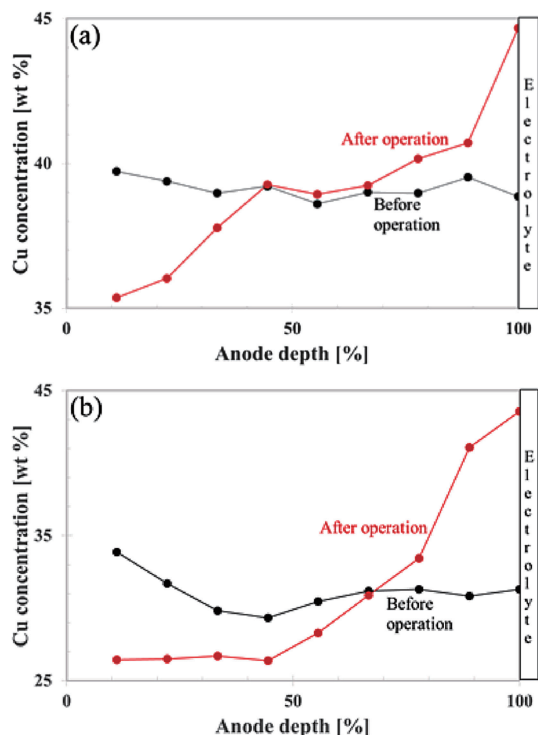


Fig. 6. Before- and after-operation Cu concentration for (a) Cu45 and (b) Cu35 anode.

$\approx +15\%$ , respectively. **Figure 6** summarizes the results collected by analysing all 9 sections in Fig. 2: here, Cu concentration is plotted as a function of the depth from the anode surface (100% depth corresponds to the electrolyte/anode interface). In both cases the migration of copper towards the electrolyte/anode interface is evident, this being responsible of Cu content reduction in the surface layers.

According to previous works, metallic atoms and/or ions can migrate in a metal/ceramic system due to grain boundary and surface diffusion phenomena.<sup>32)</sup> It is reasonable to hypothesize the diffusion and the aggregation of copper in the Cu/GDC system, even at relatively low temperature (430°C), mainly because of concentration gradients between the anode and electrolyte, as observed in previous works on Ni/YSZ-based anodic layers.<sup>33),34)</sup>

#### 4. Conclusions

Planar SOFC consisting of Li-containing GDC electrolyte and Cu-Li-GDC supporting anode were successfully fabricated by co-sintering at 900–950°C. The electrochemical characterization at 600°C revealed that it is possible to offset the ohmic resistance (caused by lower electrolyte sintering temperature) by increasing the copper content in the anode, this accounting for a larger electronic conduction. It was shown that upon the cell operation, Cu can migrate towards the electrolyte/anode interface. Such phenomenon needs additional studies to understand whether it can influence the long-term performances of the cell.

**Acknowledgements** This work was partially realized with the financial support of Caritro foundation (Cassa di Risparmio di Trento e Rovereto, Italy) by the project “Bando per progetti di ricerca scientifica nell’ambito della gestione e salvaguardia dell’ambiente, territorio e sviluppo sostenibile”. INSTM consortium is also gratefully acknowledged.

#### References

- 1) H. M. E. Rahman, S. Islam, J. H. Kim and B. T. Lee, *J. Ceram. Soc. Japan*, **117**, 1131–1133 (2009).
- 2) T. Suzuki, T. Suzuk, T. Yamaguch, H. Sumi, K. Hamamoto, Y. Fujishiro and W. Shin, *J. Ceram. Soc. Japan*, **123**, 250–252 (2015).
- 3) H. Huang, M. Nakamura, P. Su, R. Fasching, Y. Saito and F. B. Prinz, *Electrochem. Soc.*, **154**, B20–B24 (2007).
- 4) Z. Shao and S. M. Haile, *Nature*, **431**, 170–173 (2004).
- 5) N. Mahato, A. Banerjee, A. Gupta, S. Omer and K. Balani, *Prog. Mater. Sci.*, **72**, 141–337 (2015).
- 6) Y. Liu and C. G. Jiao, *Solid State Ionics*, **176**, 435–442 (2005).
- 7) C. R. He, W. G. Wang, J. Wang and Y. Xue, *J. Power Sources*, **196**, 7639–7644 (2011).
- 8) H. T. Suzuki, T. Uchikoshi, K. Kobayashi, T. S. Suzuki, T. Sugiyama, K. Furuya, M. Matsuda, Y. Sakka and F. Munakata, *J. Ceram. Soc. Japan*, **117**, 1246–1248 (2009).
- 9) D. J. L. Brett, A. Atkinson, N. P. Brandon and S. J. Skinner, *Chem. Soc. Rev.*, **37**, 1568–1578 (2008).
- 10) J. H. Nam and D. H. Jeon, *Electrochim. Acta*, **51**, 3446–3460 (2006).
- 11) E. Denkhaus and K. Salnikov, *Crit. Rev. Oncol. Hematol.*, **42**, 35–36 (2002).
- 12) M. Flytzani-Stephanopoulos, M. Sakbodin and Z. Wang, *Science*, **312**, 508–510 (2006).
- 13) D. Papurello, A. Lanzini, S. Fiorilli, F. Smeacetto, R. Singh and M. Santarelli, *Chem. Eng. J.*, **283**, 1224–1233 (2016).
- 14) H. He, R. J. Gorte and J. M. Vohs, *Electrochem. Solid-State Lett.*, **8**, A279–A280 (2005).
- 15) V. De Marco, A. Grazioli and V. M. Sglavo, *J. Power Sources*, **328**, 235–240 (2016).
- 16) A. Azzolini, V. M. Sglavo and J. A. Downs, *ECS Trans.*, **68**, 2583–2596 (2015).
- 17) V. De Marco, A. Grazioli and V. M. Sglavo, *Ceram. Eng. Sci. Proc.*, **37**, 31–38 (2016).
- 18) H. Inaba, T. Nakajima and H. Tagawa, *Solid State Ionics*, **106**, 263–268 (1998).
- 19) M. Han, Z. Liu, S. Zhou and L. Yu, *J. Mater. Sci. Technol.*, **27**, 460–464 (2011).
- 20) T. Zhu, Y. Lin, Z. Yang, D. Su, S. Ma, M. Han and F. Chen, *J. Power Sources*, **261**, 255–263 (2014).
- 21) Y. L. Liu, S. Primdahl and M. Mogensen, *Solid State Ionics*, **161**, 1–10 (2003).
- 22) V. Gil, J. Tartaj and C. Moure, *Ceram. Int.*, **35**, 839–846 (2009).
- 23) G. Accardo, C. Ferone and R. Cioffi, *Energy Technology*, **4**, 409–416 (2016).
- 24) Q. Huang, R. Hui, B. Wang and J. Zhang, *Electrochim. Acta*, **52**, 8144–8164 (2007).
- 25) Y. Zheng, C. Chen, S. Li, L. Ge, H. Chen and L. Guo, *Mater. Res. Bull.*, **46**, 130–135 (2011).
- 26) L. Zhao, X. Huang, R. Zhu, Z. Lu, W. Sun, Y. Zhang, X. Ge, Z. Liu and W. Su, *J. Phys. Chem. Solids*, **69**, 2019–2024 (2008).
- 27) P. Ried, C. Lorenz, A. Brönstrup, T. Graule, N. H. Menzler, W. Sitte and P. Holtappels, *J. Eur. Ceram. Soc.*, **28**, 1801–1808 (2008).
- 28) C. Fu, S. H. Chan, Q. Liu, X. Ge and G. Pasciak, *Int. J. Hydrogen Energy*, **35**, 301–307 (2010).
- 29) D. Montinaro, A. R. Contino, A. Dellai and M. Rolland, *Int. J. Hydrogen Energy*, **39**, 21638–21646 (2014).
- 30) R. Barfoda, M. Mogensen, T. Klemensø, A. Hagen, Y. L. Liu and P. V. Hendriksen, *J. Electrochem. Soc.*, **154**, B371–B378 (2007).
- 31) H. C. Lee and D. H. Kim, *Catal. Today*, **132**, 109–116 (2008).
- 32) Y. L. Liu and C. Jiao, *Solid State Ionics*, **176**, 435–442 (2005).
- 33) J. G. Chen, M. L. Colaianni, W. H. Weinberg and J. T. Yates, *Surf. Sci.*, **279**, 223–232 (1992).
- 34) R. J. Aaberg, R. Tunold, M. Mogensen, R. W. Berg and R. Ødegaard, *J. Electrochem. Soc.*, **145**, 2244–2252 (1998).